FINAL REPORT

U.S. Department of Energy

MECHANISM OF PITTING CORROSION PREVENTION BY NITRITE IN CARBON STEEL EXPOSED TO DILUTE SALT SOLUTIONS

Co-Principal Investigator: Philip E. Zapp

Institution: Westinghouse Savannah River Company

Co-Principal Investigator: John W. Van Zee

Institution: University of South Carolina

Project Number: SR17SP23

Grant Number: P/ID--FG07-97ER45675

Grant Project Officer: Dr. Helen Farrell

Project Duration: 9/1/97 to 12/31/01

Table of Contents

1 EXECUTIVE SUMMARY

The research has developed a broad fundamental understanding of the inhibition action of nitrite ions in preventing nitrate pitting corrosion of carbon steel tanks containing high-level radioactive waste. This fundamental understanding can be applied to specific situations during waste removal for permanent disposition and waste tank closure to ensure that the tanks are maintained safely. The results of the research provide the insight necessary to develop solutions that prevent further degradation.

The research consisted of electrochemical studies on the initiation of pitting corrosion in iron and ASTM A537 carbon steel exposed to dilute alkaline high-level radioactive waste. Nitrate and chloride are known pitting agents in this system, and nitrite is an effective inhibitor of pitting. The overall goal of this project was to develop a detailed understanding of the role of nitrite in preventing the breakdown of protective oxide on steel and on the onset of pitting, by considering the interactions of the oxidation and reduction reactions that may occur in alkaline salt solutions.

It was shown that the open circuit potential (OCP) of carbon steel ASTM537, in buffered 9.8 pH solutions, increases with increasing sodium nitrite concentration and that it decreases with increasing sodium nitrate concentration. This behavior differs from that of pure iron in that the OCP of pure iron remains almost constant in nitrite containing solutions. The OCP of both iron and carbon steel in nitrite-containing solutions reaches the steady-state value faster than in nitrate only solutions. Furthermore, the steady-state values of OCPs in nitrite solutions have fewer oscillations than in the nitrate solution. The OCP becomes noble with addition of nitrite. This reveals that nitrite functions as pitting inhibitor for carbon steel at a pH value around 9.8. Pure iron is more pitting-resistant than carbon steel at the same condition. Electrochemically, carbides function as cathodes in the presence of nitrate during pitting initiation.

Both iron and carbon steel show passivity in buffer and buffered nitrite solutions and the passive current density of carbon steel in nitrite solutions is lower than that of iron. There is no effect of NO_2^- concentration on the cyclic potentiodynamic scans of iron, but the OCP of carbon steel before scanning

increased 100 mV for 0.1 M $NaNO_2$ as compared with 0.01 M $NaNO_2$. Iron shows passivity in nitrate solutions with $NaNO_3$ concentration as high as 0.1 M, while carbon steel starts pitting in $NaNO_3$ solution at 0.01 M.

2 RESEARCH OBJECTIVES

As a result of reprocessing nuclear fuel and target elements with nitric acid, the United States Department of Energy has generated nitrate-bearing high-level radioactive waste. Much of this waste is stored in carbon steel tanks, after having been made alkaline with substantial additions of sodium hydroxide. Carbon steel is essentially immune to uniform corrosion in this environment, but it is susceptible to localized corrosion in the forms of stress corrosion cracking and pitting, depending on the temperature and the specific waste chemistry. In addition to the nitrate ion, the waste may also contain chloride and sulfate that can induce localized corrosion. The initiation of localized corrosion in the carbon steel-waste environment can be prevented by nitrite in combination with a minimum pH or hydroxide concentration.[1,2,3]

The possibility of pitting of carbon steel by the nitrate ion is a particular concern as high-level radioactive waste at the Department of Energy's Savannah River Site is diluted (washed) in preparation for its solidification in a glass waste form. Nitrate-induced pitting has therefore been extensively studied in laboratory testing of dilute (hydroxide and nitrate concentrations < 1 molar) simulated radioactive waste solutions. This work has been empirical in nature, and employed the cyclic potentiodynamic polarization (CPP) and coupon immersion techniques to identify pitting and non-pitting waste compositions. CPP scans were examined for the hysteresis in the response of the current density to the applied potential, and coupons were examined microscopically for pits. The nitrite concentration of the test solutions was varied, and the minimum nitrite concentration that prevented pitting initiation was determined. This minimum nitrite concentration was found to vary linearly with the concentration of the test solution and to depend empirically on the Celsius temperature exponentially.[3] When nitrate, chloride, or sulfate was varied independently of the other waste simulant components, the familiar linear relationship[4] was found between the logarithm of the inhibiting nitrite concentration and the logarithm of the aggressive species concentration.[2] Nitrate controls the minimum nitrite requirement to prevent pitting in certain high-level radioactive waste solutions because it is the most abundant aggressive ion in those solutions.

The overall goal of this project was to develop a detailed understanding of the role of nitrite in preventing the breakdown of protective oxide on steel and on the onset of pitting, by considering the interactions of the oxidation and reduction reactions that may occur in alkaline salt solutions. The detailed mechanism of the inhibiting action of nitrite in the presence of nitrate ions is not well understood. Indeed much of the corrosion literature is concerned with the role of chloride in the localized breakdown of passivity.[5] Considerable information concerning pitting corrosion is available for pure iron in chloride-containing solutions near pH 9, but a fundamental understanding of the role of nitrite in dilute alkaline solutions has not been reported. The goal of the project was to measure the basic pitting-related electrochemical potentials of the nitrate-nitrite-A537 carbon steel system at a pH and temperature typical of a dilute high-level waste environment (pH 9.5 to 10.5 and 40 to 50°C). Instead of complex simulants of high-level radioactive waste, the experiments employed simple alkaline solutions containing various concentrations of nitrate and nitrite. Chloride solutions were also investigated, to provide a comparison with the nitrate behavior. Open-circuit, pitting or breakdown, and some repassivation potentials were measured. The effect of nitrite on these potentials was studied by including nitrite at a concentration of 0.11 M and by eliminating nitrite from the test solutions.

3 METHODS AND RESULTS

3.1 Experimental Methods

3.1.1 ASTM A537 Steel Studies

Electrochemical potential measurements were obtained with the cyclic potentiodynamic polarization (CPP) technique, which has been the subject of recent reviews.[6,7] CPP scans were obtained with a computer-controlled potentiostat. Potential was measured with a saturated calomel electrode (SCE). The scans were started at -50 mV with respect to the open-circuit potential. The specimens were equilibrated in the heated test solutions for 5.5 hours before initiating the scan. Figure 1 shows the typical increase of the open-circuit potential with time, which continued in some instances even after 16 hours. The chosen delay of 5.5 hours allowed the collection of data in an acceptable period of time, while it permitted the specimen to

experience the substantially greater part of the approach to equilibrium. The potential was swept at a constant rate of 0.5 mV/sec and reversed upon attaining a current density of 1 mA/cm^2. The scan was terminated at 0 mV with respect to the original open-circuit potential.

All experiments were conducted with ASTM A537 class 1 carbon steel (a waste tank material of construction) discs 1.6 cm in diameter and 2.0 cm^2 of wetted surface area. A copper wire was attached with a conductive epoxy adhesive to the rear face of a disc for electrical contact, and the disc was set in an epoxy metallurgical mount. This method allowed the mounted specimen to be easily handled for grinding and polishing to a 1-micron finish. A single disc was repeatedly polished and used for many tests. The metallurgically mounted disc with a 1-micron finish is believed to yield a more consistent open-circuit potential value than that obtained with the customary 600-grit finish of a disc held in a commercial flat-specimen holder. Figure 2 shows the reproducibility obtainable in the CPP scans; the open-circuit potential for the four tests plotted varied from –63 mV to –118 mV vs. SCE.

Solutions were prepared from reagent-grade chemicals and distilled water. Sodium salts were used to introduce the nitrate, nitrite, and chloride ions. The initial pH of the solutions was set at 9.73 ± 0.05 through an equilibrium between 0.0446 M sodium bicarbonate and 0.0173 M sodium carbonate. About 500 mL of solution was used for each scan. All tests were conducted at 40°C, which is a typical storage temperature for the dilute radioactive waste. Air that had been scrubbed of carbon dioxide was bubbled through the solutions during the equilibration period and the CPP scan.

3.1.2 Commercial Purity Iron and ASTM A537 Steel Studies

Disks of commercial carbon steel ASTM537 Class 1 (0.032%Al, 0.23%C, 0.11%Cr, 1.25%Mn, 0.02%Mo, 0.08%Cu, 0.11%Ni, 0.28%Si, 0.006%P, 0.005%S, 0.003%V, Fe balance) were obtained from Metal Samples, Inc. (Munford, AL, USA). An iron rod (Goodfellow Inc., 99.99% Fe) with a diameter of 6 mm was cut into specimens with a thickness of 4 mm. The iron and carbon steel disks were mounted into epoxy resin, then polished to a 0.3 μm Al_2O_3 finish, with a grinding disk, ultrasonically cleaned in acetone, and dried in air. The exposed area was 2.0 cm^2 for carbon steel and 0.283 cm^2 for pure iron. A copper wire was attached by soldering to the rear face of the disks for electrical contact before mounting in the resin. The resin prevented crevice corrosion and allowed for grinding and polishing to a 0.3-micron finish. A pit-free smooth surface was verified at 800× for each sample at the beginning of each experiment.

For all experiments a saturated calomel reference electrode (SCE) was used. Calculations of the exposure time and flow rate from the SCE indicated that a maximum of 5 ppm Cl^- could exist in the solutions during the experiments. A graphite rod was used as a counter electrode. All recordings were obtained with a computer-controlled potentiostat (EG&G-PAR Model 263A). The cyclic potentiodynamic polarizations were performed at a scan rate of 0.5 mV/s and the scans were started at –50 mV (SCE) with respect to the open circuit potential. Before scanning, the samples were immersed for about 5.5 hours in order to obtain a stable OCP. The experiments were performed in the solutions of buffer, buffer + 0.01, 0.05, or 0.1 M $NaNO_3$, and buffer + 0.01 or 0.1 M $NaNO_2$. The buffer consisted of 0.0173 M Na_2CO_3 + 0.0446 M $NaHCO_3$ (pH 9.8 ± 0.1). The open circuit potential (OCP)-time dependence was recorded in buffered 0.1 M $NaNO_3$, buffered 0.1 M $NaNO_2$ and buffered 0.1 M $NaNO_3$, + 0.1 M $NaNO_2$ only.

Before recording the OCP, the working electrode was held at –1.0 V for 20 minutes to remove any oxide film previously formed in the air. Solutions were prepared from reagent grade chemicals and 18 MΩ deionized water. The temperature while recording OCP was kept at 40 ± 3°C. In order to remove dissolved oxygen, high purity (99.99+%) nitrogen was bubbled into the solutions. The surfaces were viewed by scanning electron microscopy to examine surface morphology at the regions between the matrix and inclusions.

3.2 Results

3.2.1 ASTM A537 Steel and Effects of Nitrate and Chloride

Figure 3 shows the CPP scans obtained from three nitrite-free solutions with the indicated nitrate

concentrations, ranging from 0.01 M to 0.3 M. As in all scans the pH was maintained at 9.73 to 9.80 and the test temperature 40 ± 2°C. These scans are typical of those obtained in the test solutions containing either nitrate or chloride as the aggressive ion.

At the lowest concentration of nitrate there is seen a wide potential range in which the A537 steel remained in a passive state, with a passive current density relatively constant at a value between 1 and 10 $\mu A/cm^2$. The current density began to increase rapidly with increasing potential (transpassive transition) at a potential of about 0.7 ± 0.1 V vs. SCE. Between 0.01 M and 0.1 M nitrate, a critical concentration of nitrate was reached that induced passive breakdown at potentials < 0.6 volts vs. SCE. (Additional testing will be performed to determine the critical concentration.) In Figure 4 the pitting potential is -0.11 V vs. SCE for 0.1 M nitrate and -0.21 V vs. SCE for 0.3 M nitrate, as determined by the potential of rapid current density increase. Further, at these concentrations a large hysteresis in current density was seen. The current density on the return portion of the scan exceeded that of the forward portion by more than an order of magnitude. Frequently, as Figure 4 shows, the repassivation potential (the potential at which the return scan current density falls below the passive current density) is lower than the original open-circuit potential. The measured open-circuit and pitting potentials in nitrate solutions without nitrite are plotted in Figure 4. Open-circuit potentials are relatively constant over the range of nitrate concentrations tested, ranging from -0.20 V to -0.35 V vs. SCE.

The addition of nitrite at a concentration of 0.11 M to the nitrate solutions has a powerful corrosion-inhibiting action on the CPP scans (Figure 5). Even at a nitrate concentration of 2.2 M, the CPP scan showed transpassive behavior and no evidence of nitrate-induced passive breakdown. The open-circuit potentials tended to increasingly negative values with the higher nitrate levels, but repeated scans continued to show a transpassive transition of about 0.75 V vs. SCE.

The higher nitrate concentrations tested did weaken the protectiveness of the passive film: the passive current density increased from about 5 $\mu A/cm^2$ to about 50 $\mu A/cm^2$ with an increase in nitrate from 0.02 to 2.2 M (Figure 6).

The CPP scans performed in chloride solutions at pH 9.73 and 40°C confirm the expectation that chloride is a much more aggressive pitting agent. Open-circuit and pitting potentials without nitrite and with 0.11 M nitrite are plotted in Figures 7 and 8, respectively, as a function of chloride concentration. The open-circuit potentials are similar to those observed in the nitrate solutions, ranging from –0.1 to –0.4 V vs. SCE. There is a tendency again to increasingly negative values with increasing aggressive ion concentration. In the nitrite-free solutions chloride induces passive breakdown at concentrations > 0.001 M, an order of magnitude lower than the comparable nitrate value. With nitrite present at 0.11 M, pitting was initiated at chloride concentrations > 0.01 M, in contrast with the steel's resistance to breakdown in the presence of 2.2 M nitrate. Pitting potentials were not determined for the highest chloride concentrations in Figure 9; the steel specimens freely corroded without achieving passivity. Chloride did not have the effect on the passive current density that nitrate did. In the chloride range 0.0001 to 0.01 M with 0.11 M nitrite present, the passive current density was essentially constant at 5 ± 3 $\mu A/cm^2$ and rose only slightly at the highest tested chloride concentrations.

For halide-induced pitting of metals, the simple relationship between pitting potential E_p and halide ion concentration C_i

$$E_p = A - B*\log C_i$$

has been determined, where A and B are constants.[8] The pitting potentials plotted in Figure 9 for chloride concentrations > 0.01 M do decrease linearly with the logarithm of chloride concentration, with the slope falling in the range reported for iron-base alloys.[9]

3.2.2 Corrosion Reactions on Iron and ASTM A537 Steel

Figure 9 shows the cyclic potentiodynamic polarizations obtained in a buffer only solution. It is found that

there is a wide potential range in which both the tested carbon steel and iron remained in the passive state (e.g., between –200 and 800mV) with a passive current density at a value at 2 ± 1 $\mu A/cm^2$. As shown in Fig. 1 the transpassive region starts at 800 mV for both metals. The passivation of both iron and carbon steel results from the formation of passive films on the sample surface, which consist of $Fe(OH)_2$ and $FeCO_3$ (at the very beginning), and Fe_3O_4 or Fe_2O_3 (at equilibrium state, see Refs. 10 and 11).

Figures 10 through 12 show the cyclic potentiodynamic polarization obtained in three buffered nitrate solutions with concentrations ranging from 0.01 M to 0.1 M. For carbon steel, in 0.01 M nitrate solution, the value of the passive current density is very similar to Fig.1. There is an increase in current density for carbon steel with potential at 325 mV that is not observed with the buffer only solution (Fig. 1). This increase in current density is attributed to the beginning of pitting. However, Fig. 10 shows that the pitting current density is limited to 20 $\mu A/cm^2$. In the solutions containing 0.05 M and 0.1 M nitrate, no passive potential region is found during the scan as the potential is increased. Visual inspection indicated that the increase in current above the OCP could be attributed to pitting of carbon steel at 0.05 M and 0.1 M $NaNO_3$. It is also seen that the open circuit potential (OCP) decreases with increasing nitrate concentration by comparing Figs. 10 through 12. This might result from the reaction of nitrate ion with the alloy elements on carbon steel. In contrast for pure iron, a passive state with a passive current density is seen in the 0.01 M and 0.05 M $NaNO_3$ solutions. In 0.1 M $NaNO_3$ only a few pits were seen on the rim of the iron coupon after polarization as might be inferred by the convergence of the positive and negative scans around –200mV vs. SCE. This suggests that pure iron has a higher pitting resistance than carbon steel. Notice that the passive current is approximately 10 times higher in 0.1 M $NaNO_3$ than in 0.01 M $NaNO_3$ for iron.

Figure 13 shows that in 0.25 M $NaNO_3$ a substantial pitting current density is observed on iron around –250 mV vs. SCE. This pitting was verified by visual observation. In 0.25M $NaNO_3$, pitting occurred on carbon steel as soon as it was immersed and therefore those data are not shown in Fig. 13. Figure 14 shows the cyclic potentiodynamic polarization scan of pure iron and carbon steel in buffered 0.1 M $NaNO_3$ + 0.1 M $NaNO_2$ solutions. There was no pitting observed for either metal. All these results strongly suggest nitrite can prevent A537 carbon steel from pitting in simple alkaline solution as it does in the complex solutions of Ref. 3.

Figures 15 and 16 show the behavior in buffered $NaNO_2$ solutions free of $NaNO_3$. The behavior of iron is similar to that in nitrate solutions. However, the carbon steel now is more passive than iron. Also there is no effect of NO_2^- concentration on the scans. The passive current densities are within approximately 0.2 $\mu A/cm^2$ which are much lower than those in the buffered nitrate solutions. This is probably because different passive films are formed on the working electrode surfaces in NO_2^- and NO_3^- solutions. For example, it has been reported that nitrite can react with ferrous ion to form Fe_2O_3 [12] It could also be that the film on carbon steel in NO_2^- is less porous than in NO_3^-. Either a different film or a more porous film could contribute to the fact that the transpassive region starts about 100 mV lower in 0.01 M NO_2^- solutions than in 0.01 M NO_3^- solutions. The OCPs shown after the reverse scan are about 200 mV higher than those before scanning in contrast to only about 100 mV higher in NO_3^- solutions at 0.01 M. This implies nitrite is a good inhibitor for carbon steel at this pH. It is also seen that the OCP before scanning increased 100 mV for 0.1M NO_2^- as compared with 0.01 M NO_2^-. Thus the inhibition behavior of nitrite is related to concentration as shown in Ref. 13. Reference 13 stated that carbon steel in 0.11M nitrite solution retained passivity in solution even at a nitrate concentration of 2.2M.

3.2.3 Open Circuit Potential Measurements and Corrosion Reactions

In this section we present measurements of changes in the open circuit potential from initial immersion to a steady state. These data reflect the formation of passive films. The change in OCP with time is shown in Figs. 17 through 19 for a buffered 0.1 M $NaNO_3$ solution, a buffered 0.1 M $NaNO_2$ solution, and a buffered solution containing 0.1 M $NaNO_3$ and 0.1 M $NaNO_2$, respectively. These show that the carbon steel electrode exhibits significantly different equilibrium when NO_2^- is absent. In the solution of buffer and 0.1 M $NaNO_3$, the OCP-time profile may be divided into three stages as shown in Fig.17. In stage I, the OCP increases slowly to –720 mV from –780 mV, and then it rises to a stable value of –480 mV at 600 min. after immersion. This might be attributed to the following four reactions as discussed in Refs. 14 and 15:

$$Fe + NO_3^- + H_2O \rightarrow Fe(OH)_2 + NO_2^- \quad (1)$$

$$3Fe(OH)_2 + NO_3^- \rightarrow Fe_3O_4 + NO_2^- + 3H_2O \quad (2)$$

$$Fe_3O_4 + 2H_2O + NO_2^- \rightarrow 3FeOOH + NO + OH^- \quad (3)$$

$$2Fe_3O_4 + 2NO_2^- + H_2O \rightarrow 3Fe_2O_3 + 2NO + 2OH^- \quad (4)$$

At the start, the fresh surface is mainly Fe since it was held for 20 min. at –1.0 V before recording OCP. Then the Fe was oxidized first to $Fe(OH)_2$ and then to Fe_3O_4 by nitrate. Finally Fe_3O_4 might be oxidized to FeOOH or Fe_2O_3, which are more stable, as nitrite is reduced. The half reactions for reaction 1-4 can be written:

$$NO_3^- + H_2O + 2e^- \rightarrow NO_2^- + 2OH^- \quad (1\text{-a})$$

$$Fe + 2OH^- \rightarrow Fe(OH)_2 + 2e^- \quad (1\text{-b})$$

$$NO_3^- + H_2O + 2e^- \rightarrow NO_2^- + 2OH^- \quad (2\text{-a})$$

$$3Fe(OH)_2 + 2OH^- \rightarrow Fe_3O_4 + 4H_2O + 2e^- \quad (2\text{-b})$$

$$NO_2^- + H_2O + e^- \rightarrow NO + 2OH^- \quad (3\text{-a})$$

$$Fe_3O_4 + H_2O + OH^- \rightarrow 3FeOOH + e^- \quad (3\text{-b})$$

$$NO_2^- + H_2O + e^- \rightarrow NO + 2OH^- \quad (4\text{-a})$$

$$2Fe_3O_4 + 2OH^- \rightarrow 3Fe_2O_3 + H_2O + 2e^- \quad (4\text{-b})$$

In fact, the corrosion products are determined not only by the thermodynamic relationship but also by the kinetics of corrosion. The transients in these figures may be related to the kinetics.

As shown in Figure 17 for carbon steel during stage II, the potential rise is approximately linear with time indicating that the thickness of passive film is growing. This implies that neither the anodic or cathodic fluxes nor concentration is the limiting process.[16] The thickness of passive film keeps growing until 720 min. After immersion for 720 min the linear increase in the potential stops and gradually diminishes to a steady-state value. This suggests some other step associated with either the anodic or cathodic process becomes rate-controlling.[17] Even though the corrosion potential reaches a relatively stable value of –480 mV vs. SCE, the oscillations in OCP indicate some pitting occurs on carbon steel during stage III. For pure iron in the same buffered 0.1M $NaNO_3$, there are only two stages in the OCP-time curve. It is assumed that the surface film in stage I is the same as that on the carbon steel surface, and remains unchanged until 330 min. After 330 min, it changes quickly to FeOOH or Fe_2O_3. Also the stable OCP of pure iron has fewer oscillations than carbon steel. As shown in the potentiodynamic polarization scan (e.g., see Fig. 12), the iron samples remain passive until 800 mV. The occurrence of pitting on carbon steel and the lack of pitting on iron suggest that the carbide inclusions and alloy elements facilitate pitting.

Figure 18 and 19 compare the OCP-time relationships when $NaNO_2$ is present. For these figures we divide the behavior into five regions. Region I is longer when $NaNO_3$ is present (e.g., compare Fig. 19 with Fig. 18), and it is much shorter than when $NaNO_2$ is present (e.g., compare Fig. 17 and Fig. 19). We believe this short period is due to the rapid kinetics for NO_2^- reduction, perhaps according to reaction (5) on the fresh iron and $Fe(OH)_2$ surfaces. Thus

$$2Fe(OH)_2 + 2NO_2^- \rightarrow Fe_2O_3 + 2NO + 2OH^- + H_2O \quad (5)$$

the half reaction can be written:

$$NO_2^- + H_2O + e^- \rightarrow NO + 2OH^- \quad (5\text{-a})$$

$$Fe(OH)_2 + 2OH^- \rightarrow Fe_2O_3 + 3H_2O + 2e^- \quad (5\text{-b})$$

As shown in Fig.19, in buffered 0.1 M $NaNO_3$/0.1 M $NaNO_2$ solutions, the OCP-time relationship of

carbon steel may be divided into five stages. We suggest the following additional reaction is involved:

$$2FeOOH \rightarrow Fe_2O_3 + H_2O \qquad (6)$$

In the first stage, Fe is oxidized to $Fe(OH)_2$ (Ref. 18 see Reaction 1) and the $Fe(OH)_2$ is quickly oxidized by NO_2^- because nitrite has a strong chemical oxidization potential in alkaline solution according to reaction (5). Iron shows a similar behavior to carbon steel except the life span of $Fe(OH)_2$ in stage I is longer and the life span of Fe_3O_4 in stage II is shorter. These differences in time are probably due to the presence of carbides in the surface of carbon steel, which function as local cathodes and facilitate the reaction between NO_2^- and Fe or $Fe(OH)_2$. However, the reason for the shorter life span of Fe_3O_4 in stage II in iron is unknown. In buffered 0.1 M $NaNO_2$, the evolution of the passive films on carbon steel and iron are very similar to those in 0.1 M $NaNO_2$ + 0.1 M $NaNO_3$ except the stage II of pure iron is again shorter. As shown in the Pourbaix diagram of iron in buffer solution of Ref. 19, Fe_2O_3 exists at more noble potentials while FeOOH exists at relatively low potentials. However, both of them exist at the passive state of the steel.[20]

Figures 20 and 21 reorganized the data of Figs. 17 through 19 to show a comparison of the effect of solutions on carbon steel and iron respectively. In Fig. 20, the OCP of carbon steel in a 0.1 M $NaNO_3$ solution increases slowly to a steady value (line number 3), while it increases sharply in a 0.1 M $NaNO_2$ solution (line number 2) to a constant value. By comparing line 1 and line 2, it is found that the OCP of carbon steel increases faster in 0.1M $NaNO_2$ than in 0.01 M $NaNO_2$ and the OCP is also higher. The final OCP increases with the addition of nitrite and decreases with the addition of nitrate. Figure 21 shows that the OCP of pure iron remains almost a constant in buffer solution. This implies the composition of the passive film in buffer did not change. Raman spectroscopy revealed it consists of $FeCO_3$.[21] In 0.1 M $NaNO_3$ solution (line 3), there are only two stages in the OCP-time curve and it suggests only two kinds of species appeared during immersion, probably $Fe(OH)_2$ and Fe_2O_3. There are three stages in the OCP-time curves in nitrite containing solutions, and this reveals that there are probably three kinds of species appeared during immersion, probably $Fe(OH)_2$, FeOOH, and Fe_2O_3. In Fig. 21, the OCP of pure iron remains at –0.77 V for almost 130 hours in 0.01 M $NaNO_2$ (line 1) while it increases to –0.4 V after immersed 12 hours in 0.1 M $NaNO_2$ (line 2). This implies that NO_2^- reacts with iron and the higher concentration of NO_2^-, the faster the reaction occurs. By comparison of Fig.20 with 21, it is found that the OCP of pure iron is more stable than the carbon steel in NO_3^- containing solutions.

4 CONCLUSIONS

An electrochemical study has been initiated on the initiation of pitting corrosion in ASTM A537 carbon steel exposed to dilute alkaline high-level radioactive waste. Nitrate and chloride are known pitting agents in this system, and nitrite is an effective inhibitor of pitting. The effects on the open-circuit and pitting potentials of the two aggressive ions in the presence and absence of nitrite have been examined independently at a pH of 9.73 (buffered by sodium bicarbonate and sodium carbonate) and a temperature of 40°C.

It was shown that the open circuit potential (OCP) of carbon steel ASTM537, in buffered 9.8 pH solutions, increases with increasing sodium nitrite concentration and that it decreases with increasing sodium nitrate concentration. This behavior differs from that of pure iron in that the OCP of pure iron remains almost constant in nitrite containing solutions. The OCP of both iron and carbon steel in nitrite-containing solutions reaches the steady-state value faster than in nitrate only solutions. Furthermore, the steady-state values of OCPs in nitrite solutions have fewer oscillations than in the nitrate solution. The OCP becomes noble with addition of nitrite. This reveals that nitrite functions as pitting inhibitor for carbon steel at a pH value around 9.8. Pure iron is more pitting-resistant than carbon steel at the same condition. Electrochemically, carbides function as cathodes in the presence of nitrate during pitting initiation.

Both iron and carbon steel show passivity in buffer and buffered nitrite solutions and the passive current density of carbon steel in nitrite solutions is lower than that of iron. There is no effect of NO_2^- concentration on the cyclic potentiodynamic scans of iron, but the OCP of carbon steel before scanning increased 100 mV for 0.1 M $NaNO_2$ as compared with 0.01 M $NaNO_2$. Iron shows passivity in nitrate solutions with $NaNO_3$ concentration as high as 0.1 M, while carbon steel starts pitting in $NaNO_3$ solution at 0.01 M.

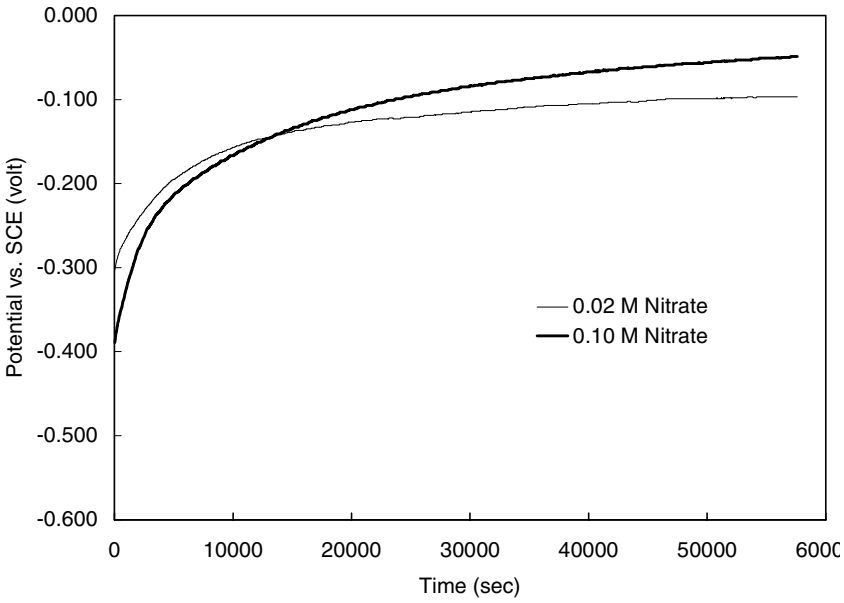

Figure 1. Variation of the open-circuit potential of the steel specimen with time for two nitrate concentrations. Nitrite concentration 0.11 M, pH 9.73, temperature 40°C.

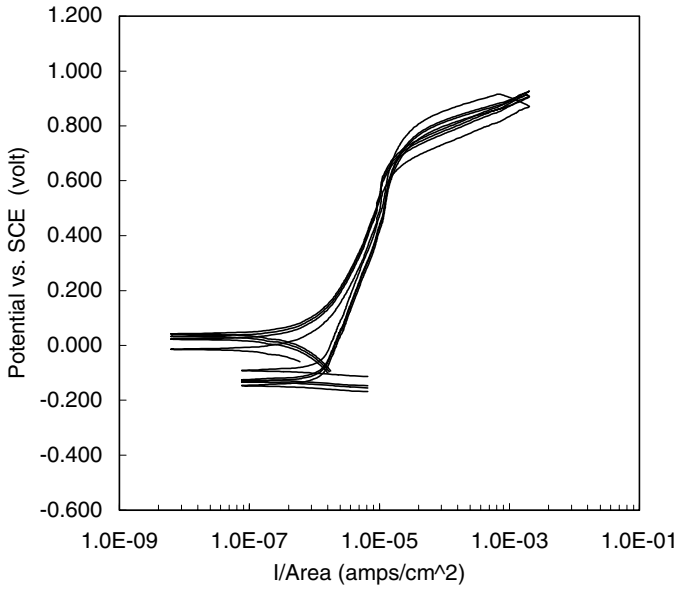

Figure 2. Four cyclic potentiodynamic polarization scans at 0.02 M nitrate and 0.11 M nitrite.

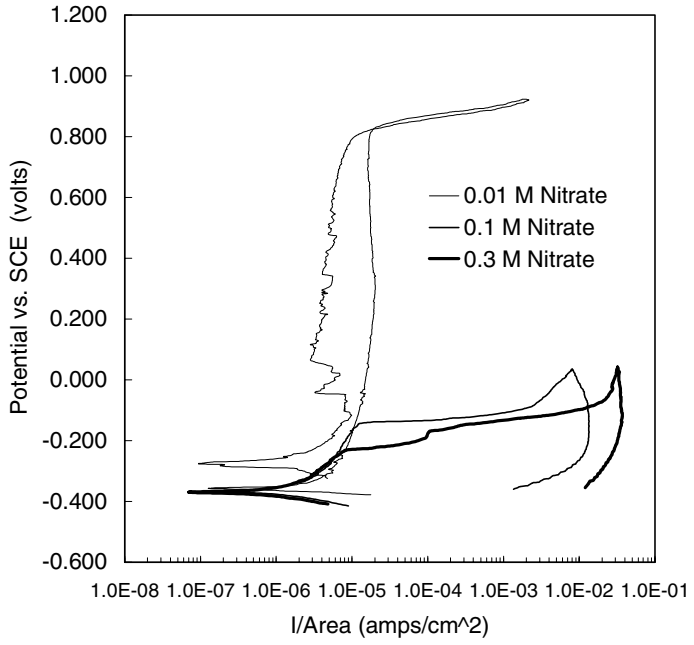

Figure 3. Cyclic potentiodynamic polarization scans in solutions with indicated nitrate concentrations and no nitrite, showing the onset of pitting with nitrate between 0.1 and 0.3 M nitrate.

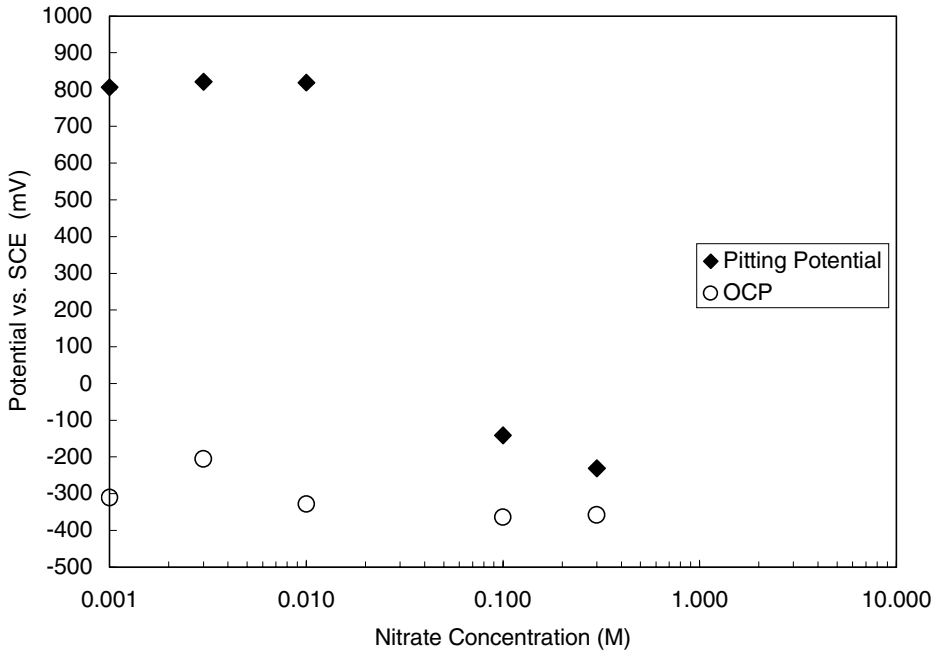

Figure 4. Variation of open-circuit (OCP) and pitting potentials with nitrate concentration at pH 9.73 and 40°C with no nitrite present.

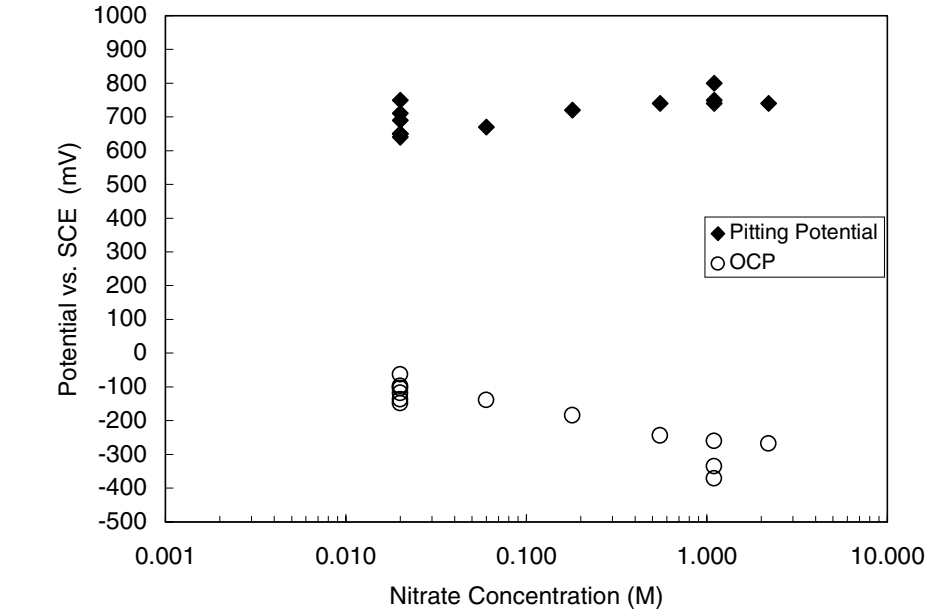

Figure 5. Variation of open-circuit and pitting potentials with nitrate concentration at pH 9.73 and 40°C with 0.11 M nitrite present.

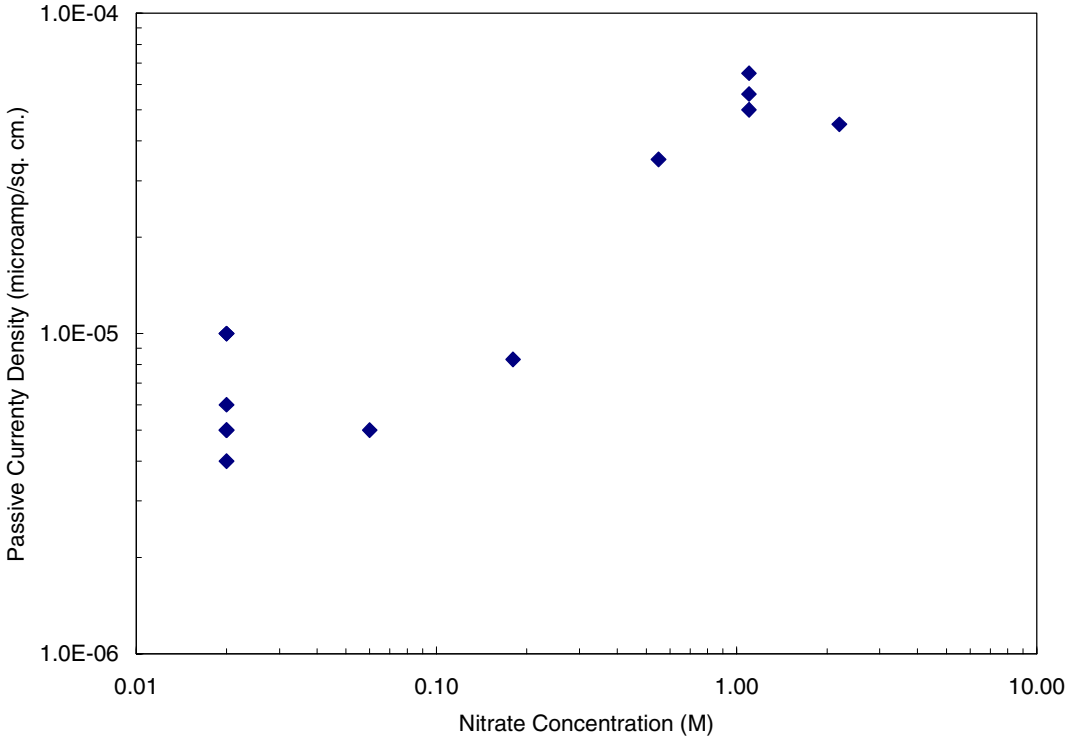

Figure 6. Variation of passive current density with nitrate concentration in solutions with 0.11 M nitrite present.

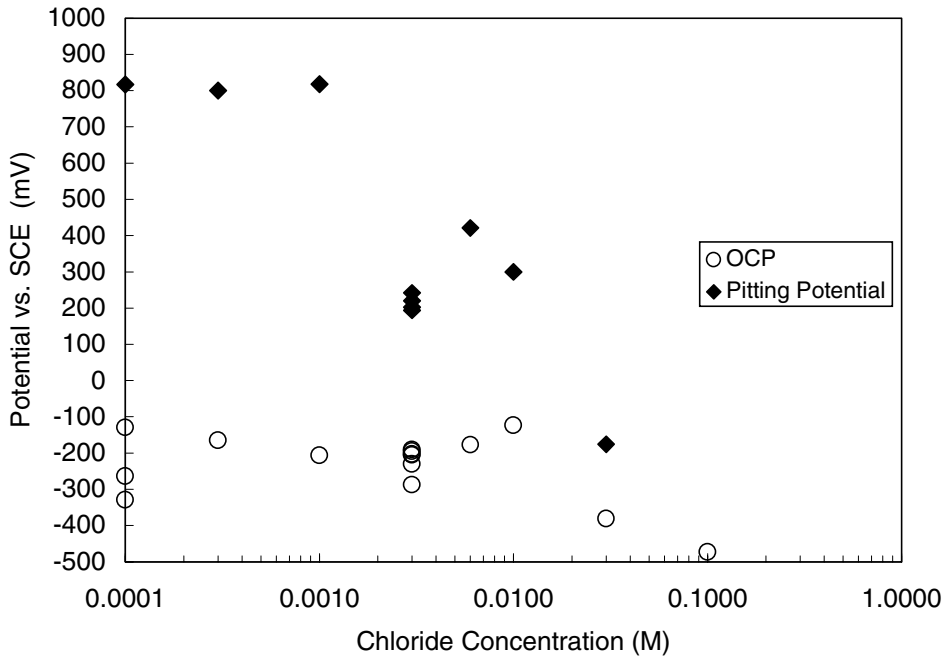

Figure 7. Variation of open-circuit and pitting potentials with chloride concentration at pH 9.73 and 40°C with no nitrite present.

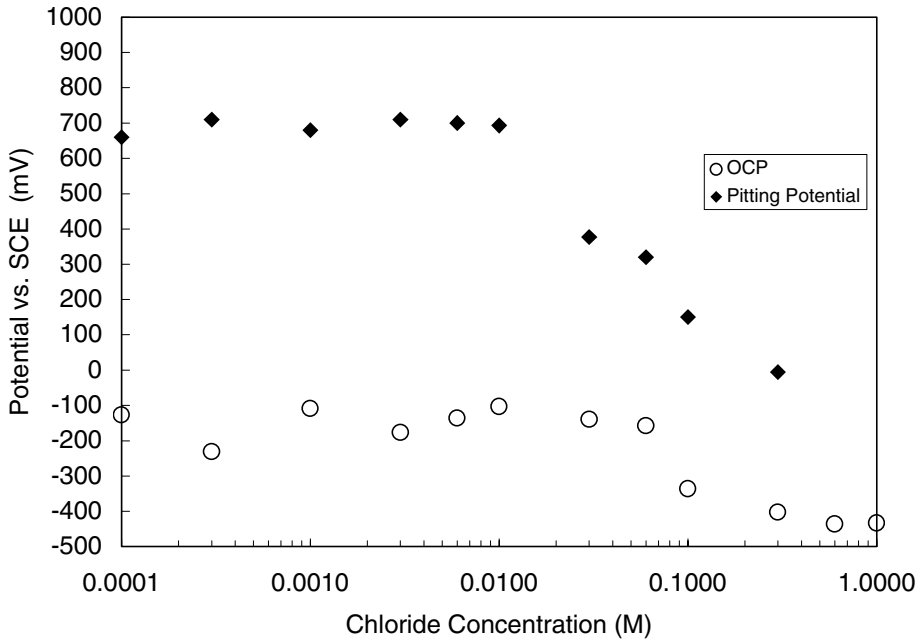

Figure 8. Variation of open-circuit and pitting potentials with chloride concentration at pH 9.73 and 40°C with 0.11 M nitrite present.

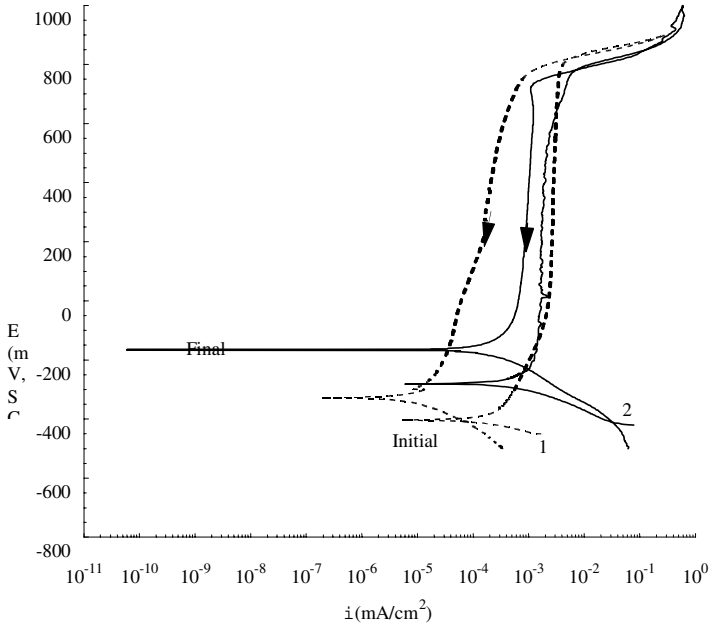

Figure 9. Comparison of cyclic potentiodynamic polarization scans for pure iron (1, dash line) and carbon steel (2, solid line) in buffer solution. The arrow indicates the direction of the scan and 'Initial' indicates the rest potential as the potential is increased from -50 mV of the OCP and 'Final' indicates the rest potential in the reverse scan.

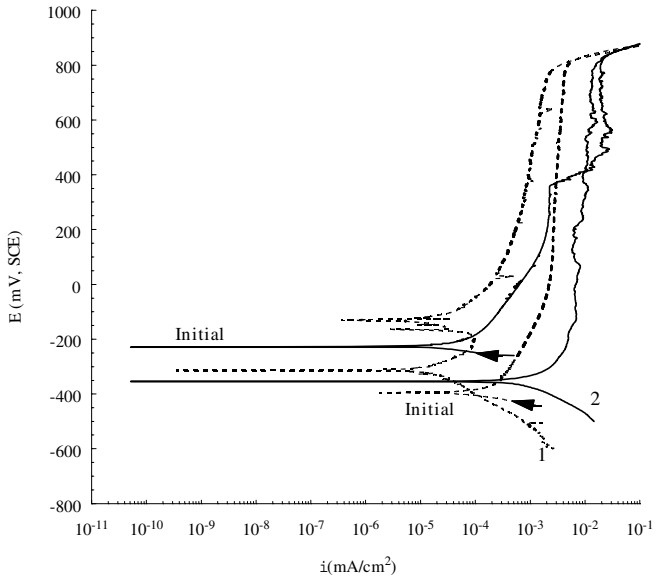

Figure 10. Comparison of cyclic potentiodynamic polarization scans in buffered 0.01 M $NaNO_3$ for pure iron (1, dash line) and carbon steel (2, solid line) . The arrow indicates the direction of the scan and 'Initial' indicates the rest potential as the potential is increased from -50 mV of the OCP.

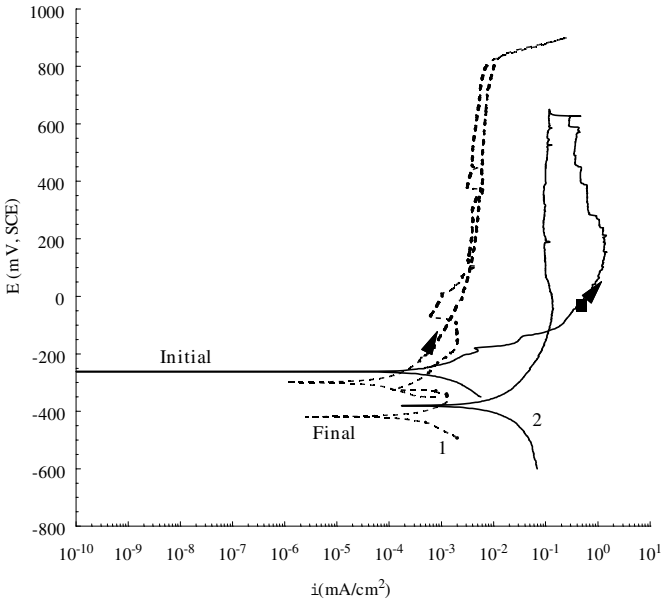

Figure 11. Comparison of cyclic potentiodynamic polarization scans for pure iron (1, dash line) and carbon steel (2, solid line) in buffered 0.05 M $NaNO_3$ solution. The arrow indicates the direction of the scan and 'Initial' indicates the rest potential as the potential is increased from -50 mV of the OCP and 'Final' indicates the rest potential in the reverse scan.

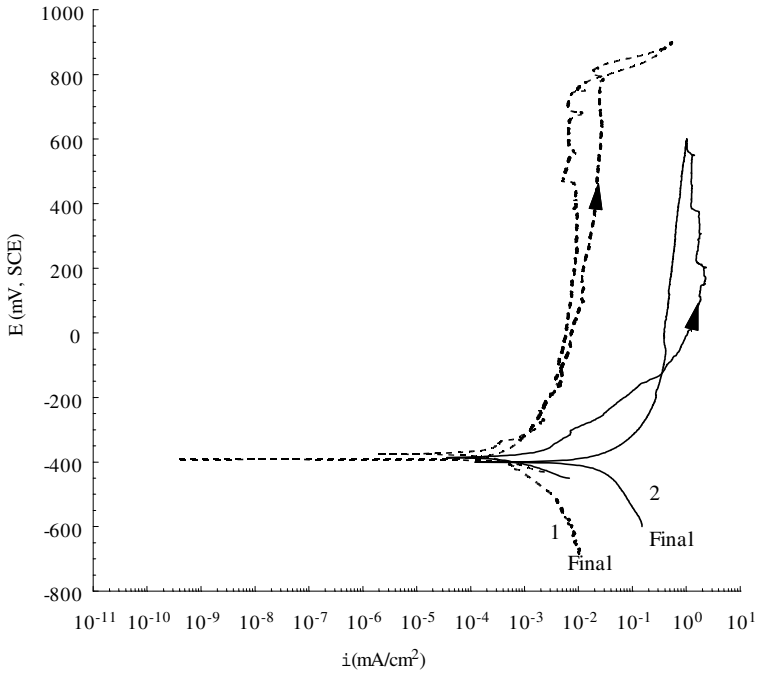

Figure 12. Comparison of cyclic potentiodynamic polarization scans in buffered 0.1 M $NaNO_3$ for pure iron (1, dash line) and carbon steel (2, solid line). The arrow indicates the direction of the scan and 'Final' indicates the rest potential in reverse scan.

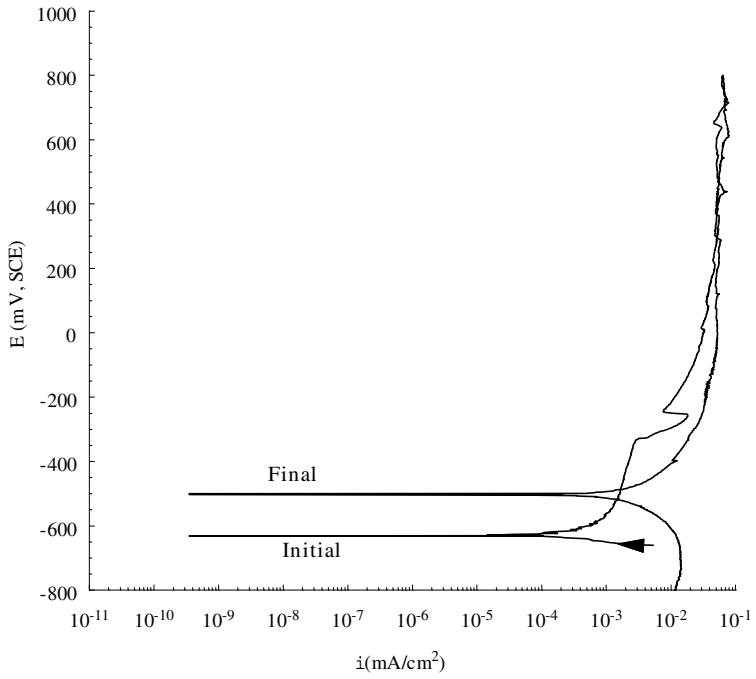

Figure 13. Cyclic potentiodynamic polarization scans in buffered 0.25 M $NaNO_3$ for pure iron. The arrow indicates the direction of the scan and 'Initial' indicates the rest potential as the potential is increased from -50 mV of the OCP and 'Final' indicates the rest potential in the reverse scan.

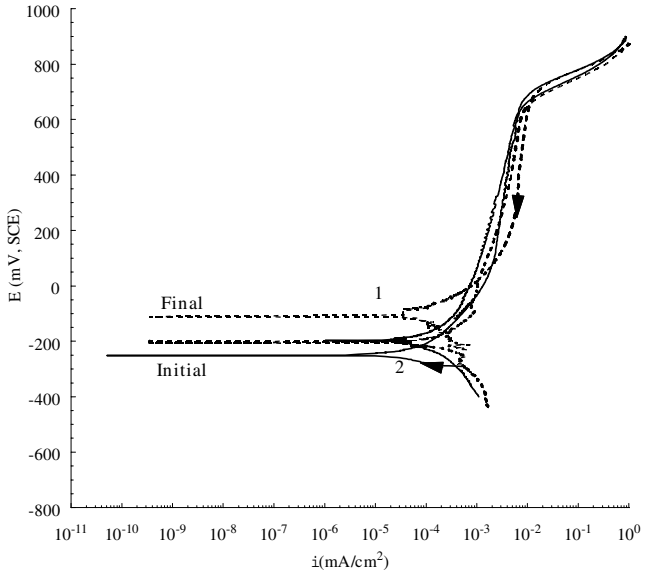

Figure 14. Comparison of cyclic potentiodynamic polarization scans in buffered 0.1 M $NaNO_3$ + 0.1 M $NaNO_2$ for pure iron (1, dash line) and carbon steel (2, solid line). The arrow indicates the direction of the scan and 'Initial' indicates the rest potential as the potential is increased from -50 mV of the OCP and 'Final' indicates the rest potential in the reverse scan.

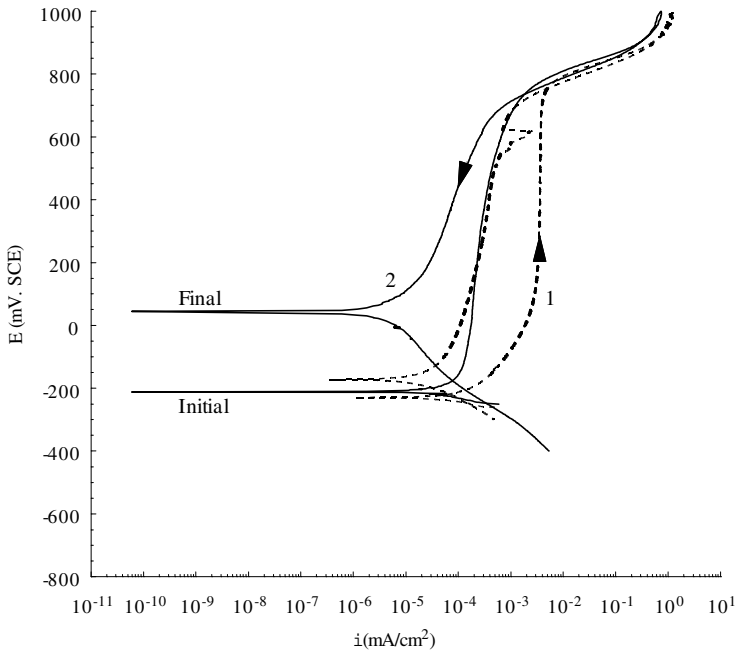

Figure 15. Comparison of cyclic potentiodynamic polarization scans in buffered 0.01 M $NaNO_2$ for pure iron (1, dash line) and carbon steel (2, solid line). The arrow indicates the direction of the scan and 'Initial' indicates the rest potential as the potential is increased from -50 mV of the OCP and 'Final' indicates the rest potential in the reverse scan.

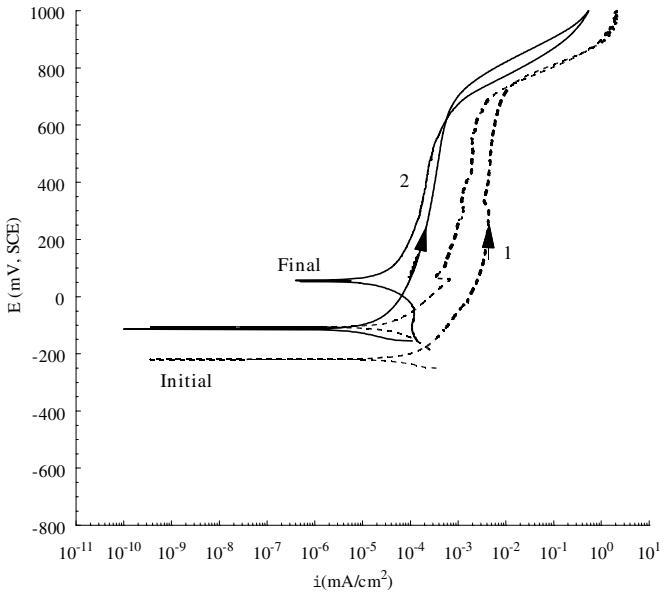

Figure 16. Comparison of cyclic potentiodynamic polarization scans in buffered 0.1 M $NaNO_2$ for pure iron (1, dash line) and carbon steel (2, solid line).

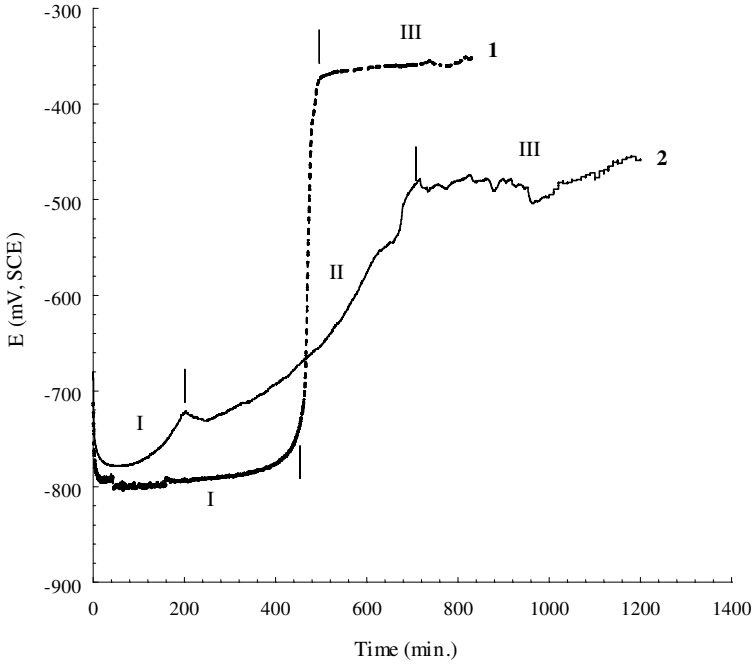

Figure 17. Comparison of the changes in the open circuit potential (OCP) for pure iron (1, dash line) and carbon steel (2, solid line) after immersion in buffered 0.1M $NaNO_3$ solution. The Roman numerals indicate regions in which different reactions occur as discussed in the text.

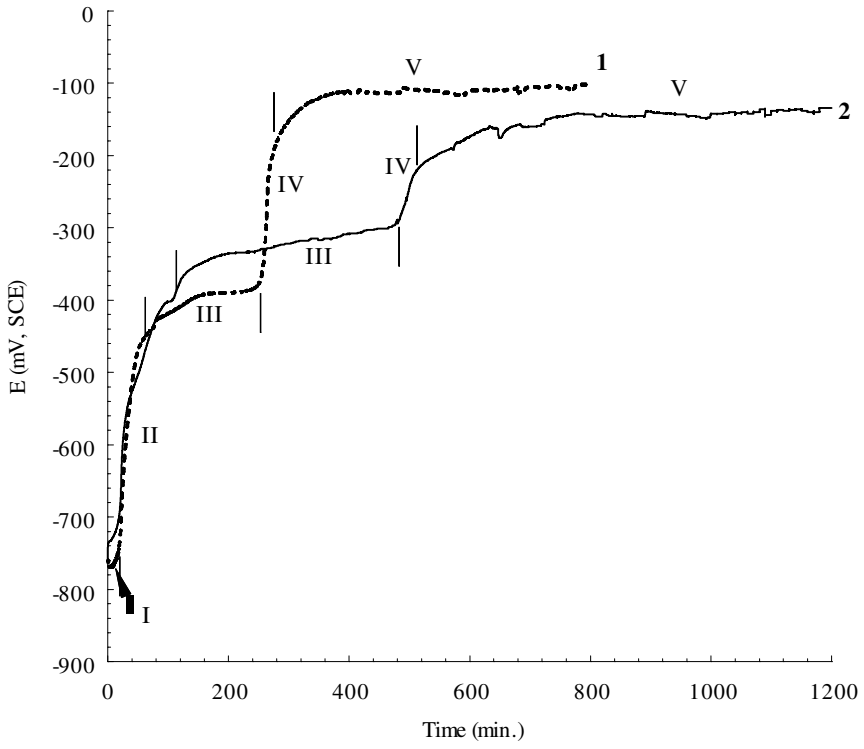

Figure 18. Comparison of the changes in the open circuit potential (OCP) for pure iron (1, dash line) and carbon steel (2, solid line) after immersion in a buffered 0.1M $NaNO_2$ solution. The Roman numerals indicate regions in which different reactions occur as discussed in the text.

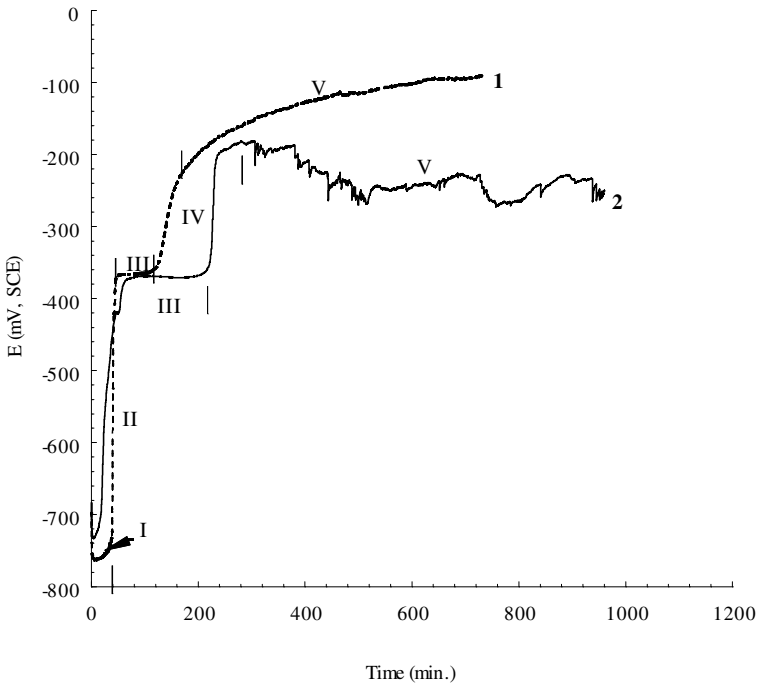

Figure 19. Comparison of the changes in the open circuit potential (OCP) for pure iron (1, dash line) and carbon steel (2, solid line) after immersion in a buffered 0.1M $NaNO_3$ + 0.1M $NaNO_2$ solution. The Roman numerals indicate regions in which different reactions occur as discussed in the text.

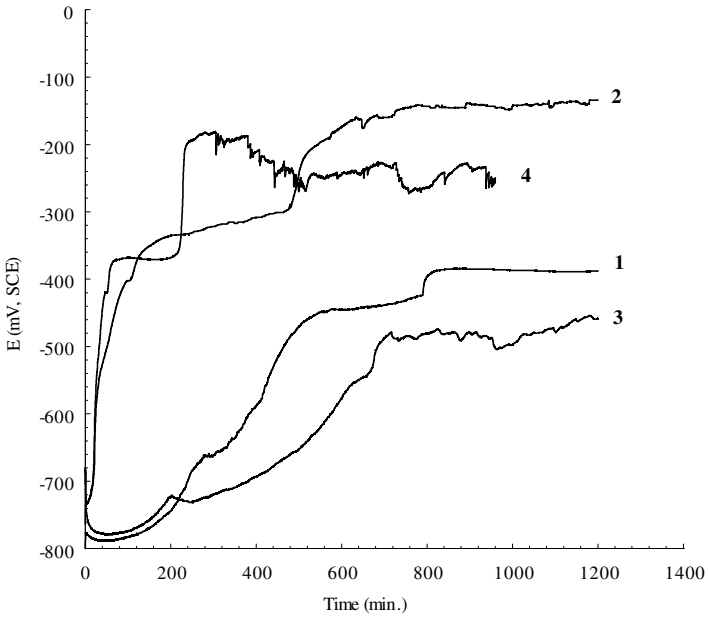

.

Figure 20. The effect of NO_2^- and NO_3^- on the OCP-time of ASTM537 carbon steel. Legend: 1 = 0.01M $NaNO_2$; 2 = 0.1M $NaNO_2$; 3 = 0.1M $NaNO_3$; 4 = 0.1M $NaNO_2$ + 0.1M $NaNO_3$; all solutions contain buffer.

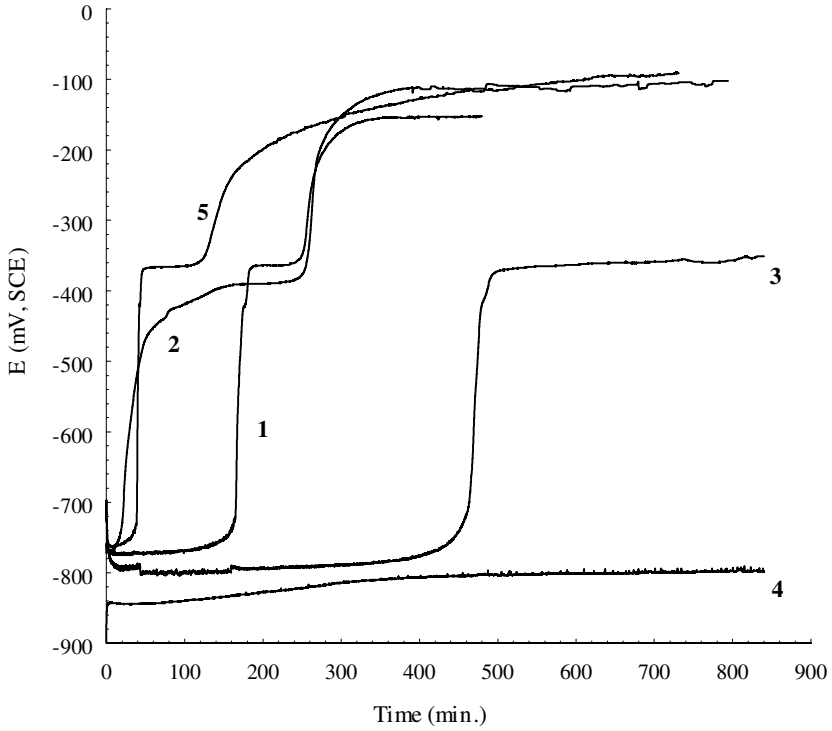

Figure 21. The effect of NO_2^- and NO_3^- on the OCP-time of pure iron. Legend: 1 = 0.01M $NaNO_2$; 2 = 0.1M $NaNO_2$; 3 = 0.1M $NaNO_3$; 4 = buffer only; 5 = 0.1M $NaNO_2$ + 0.1M $NaNO_3$; all solutions contain buffer.

5 RELEVANCE, IMPACT AND TECHNOLOGY TRANSFER

The high level waste tanks are a critical element of the SRS and Hanford high level waste management program. The current DOE high-level waste system flow sheet uses the carbon steel high level waste tanks beyond the year 2035. Hence the life management of these tanks well beyond the 40-year design lifetime of typical carbon steel structures is a key element to successful implementation of the high-level waste system flow sheet both at SRS and Hanford. The assessment of the degradation of these tanks is a key input into tank structural integrity analysis and the tank life management programs. The primary degradation mechanisms are pitting and stress corrosion cracking. A detailed understanding of these mechanisms is hence required to develop the basis for demonstrating tank structural integrity and successful life management for the next 10-30 years. Current understanding of pitting in carbon steel tanks containing high level waste is limited to identifying the environmental conditions for pit initiation. The EMSP program detailed in this report extends this understanding to the growth of pits, i.e. the kinetics of pitting, in carbon steel tanks in the high level waste environment. Data and models on pitting kinetics are necessary both to predict potential for tank leaks by this mechanism. The fact that pitting is a random process makes development of a comprehensive model a major challenge but the payback of a successful model is significant both in terms of increased tank lifetime and avoidance of unanticipated events. The proposed pitting kinetics can be readily adapted and transferred through the tank farm management through incorporation in the Technical Safety Standards.

The research has also developed a broad fundamental understanding of the inhibition action of nitrite ions in preventing nitrate pitting. This fundamental understanding can be applied to specific situations during waste removal and closure to ensure that the tanks are maintained safely. The results of the research provide the insight necessary to develop solutions that prevent further degradation. Further degradation, if not prevented, can adversely affect the closure process by reducing acceptable tank fill limits, forcing unanticipated waste transfers, minimizing the efficiency of waste contents. Ultimately, newly found degradation may require the reduction of safety margins to meet the current site-specific baselines for waste processing, and tank closure.

6 PROJECT PRODUCTIVITY

The principal goals of the project were realized.

7 PERSONNEL SUPPORTED

7.1 Savannah River Technology Center

Philip E. Zapp, PI

7.2 University of South Carolina

John W. Van Zee, PI
Lifeng Chen, Graduate Student
Xuebing Huang, Post-doc

8 PUBLICATIONS

Reviewed Publications: P.E. Zapp and J.W. Van Zee, *Corrosion/99*, Paper No.471, NACE International, Houston, TX, 1999.

Submitted to Peer-Reviewed Journals: Xuebing Huang, Lifeng Chen, John W. Van Zee, and Philip E. Zapp, "Comparison of Pitting Corrosion on Iron and ASTM537 Carbon Steel in Alkaline Nitrate/Nitrite Solutions," submitted to *Corrosion Science*, 2001.

9 INTERACTIONS

The work described in this Final Report has been presented and discussed in both formal symposia and informal committee meetings of the National Association of Corrosion Engineers, the American Institute of Chemical Engineers, and The Electrochemical Society. The work has been discussed as part of Savannah River Site presentations at the Workshop on Recommendations for Hanford Double-Shell Tank Life Extension, Richland, Washington, May 1-4, 2001, Charles W. Stewart, Pacific Northwest National Laboratory, workshop chairman.

10 TRANSITIONS

Localized corrosion, of which pitting corrosion is a critical and prominent example, is the principal historical degradation mode of carbon-steel, high-level radioactive waste tanks at the Savannah River Site. The work discussed in this Final Report will be used to further develop the understanding and mitigation of all forms of localized corrosion. Specifically at the Savannah River Site, localized corrosion modes in the steel in contact with the vapor or headspace over the waste in partially filled tanks has become an emergent issue in older, non-stress-relieved tanks, which are potentially subject to another form of localized corrosion known as stress corrosion cracking. It is believed that corrosion reactions similar to those discussed in Section 3 above participate at the active tips of stress corrosion cracks, while the crack side walls become repassivated. As discussed below in Section 12, this corrosion mode as well as pitting corrosion are suspected to be active in vapor space corrosion and will be investigated in 2002 at the Savannah River Technology Center. The High-Level Waste Division, Westinghouse Savannah River Co., will support this work at the Savannah River Site. The Tanks Focus Area (and successors) as well as the EMSP will be kept informed of the progress of this work.

11 PATENTS

None.

12 FUTURE WORK

The project is leading to future work in the area of localized corrosion and its mitigation in steel that is in contact not with the bulk liquid waste but rather with the vapor above that liquid, in partially filled waste tanks. Experiments are to be initiated in FY2002 to study pitting corrosion and stress corrosion cracking in the vapor conditions.

13 LITERATURE CITED

1. R. S. Ondrejcin, S. P. Rideout, and J. A. Donovan, “Control of Stress Corrosion Cracking in Storage Tanks Containing Radioactive Waste,” *Nuclear Technology* 44, p. 297 (1979).

2. J. W. Congdon, “Inhibition of Nuclear Waste Solutions Containing Multiple Aggressive Anions,” *Materials Performance 15*, p. 34 (1988).

3. P. E. Zapp and D. T. Hobbs, “Inhibiting Pitting Corrosion in Carbon Steel Exposed to Dilute Radioactive Waste Slurries,” CORROSION/92, paper no. 98, (Houston, TX: NACE International, 1992).

4. S. Matsuda and H. H. Uhlig, *J. Electrochem. Soc.* 111, p. 156 (1964).

5. Z. Szklarska-Smialowska, *Pitting Corrosion of Metals* (Houston, TX: National Association of Corrosion Engineers, 1986).

6. D. C. Silverman, “Tutorial on Cyclic Potentiodynamic Polarization Technique,” CORROSION/98, paper no.299, (Houston, TX: NACE International, 1998).

7. J. A. Beavers, C. L. Durr, N. G. Thompson, "Unique Interpretations of Potentiodynamic Polarization Technique," CORROSION/98, paper no.300, (Houston, TX: NACE International, 1998).

8. Z. Szklarska-Smialowska, "Inhibition of Pitting Corrosion," CORROSION/89, paper no. 140, (Houston, TX: NACE International, 1989).

9. Reference 5, p. 204.

10. Y. Xu, M.H. Wang, and H.W. Pickering, *J. Electrochem. Soc*., **140** (1993), No.12, pp.3448-3457.

11. C. Gabrielli, F. Huet, M. Keddam, and R. Oltia, *Advances in Localized Corrosion*, in: H. Isaacs, U. Bertocci, J. Kruger, and Z. Szklarska-Smialowska (Eds.), Houston, TX, 1990, p93.

12. D.C. Cook, A.C. Van Orden, J.J. Carpio, and S.J. Oh, *Hyperfine Interactions*, **113** (1998), pp.319-329.

13. P.E. Zapp and J.W. Van Zee, *Corrosion/99*, Paper No.471, NACE International, Houston, TX, 1999.J.W. Congdon, *Corrosion/88,* Paper no. 274, NACE International, Houston, TX, 1988.

14. S.J. Oh, D.C. Cook, and H.E. Townsend, *Hyperfine Interactions*, **112** (1998), pp.59-65.

15. L.J. Oblonsky and T.M. Devine, *Corr. Sci*., **37** (1995), No.1, pp.17-44.

16. M.S. Odziemkowski, T.T. Schuhmacher, R.W. Gillam, and E.J. Reardon, *Corr. Sci*., **40** (1998), No.2/3, pp.371-389.

17. T.E. Evans, *Corr. Sci*., **17** (1977), pp.105.

18. J. Gui and T.M. Devine, *J. Electrochem. Soc*., **138** (1991), No.5, pp.1376-1384.

19. Ph. Refait and J.M.R. Génin, *Corr. Sci*., **34** (1993), No.5, pp.797-819..

20. D.W. Buzza and R.C. Alkire, *J. Electrochem. Soc*., **142** (1995), No.4, pp.1104-1111.

21. J.C. Rubin and J. Dunnward, *J Electroannal. Chem.,***258** (1989), pp.327-344.